HHS Public Access

Author manuscript

Oncogene. Author manuscript; available in PMC 2021 April 19.

Published in final edited form as:

Oncogene. 2020 November ; 39(46): 6961–6974. doi:10.1038/s41388-020-01511-9.

A cell-penetrating MARCKS mimetic selectively triggers cytolytic death in glioblastoma

Nicholas J. Eustace[1], **Joshua C. Anderson**[1], **Jason M. Warram**[2], **Hayley N. Widden**[3], **Rune T. Pedersen**[6], **Hasan Alrefai**[1], **Zeel Patel**[1], **Patricia H. Hicks**[1], **William J. Placzek**[3], **G. Yancey Gillespie**[4], **Anita B. Hjelmeland**[5], **Christopher D. Willey**[1]

[1]Department of Radiation Oncology, The University of Alabama at Birmingham, Birmingham Alabama

[2]Department of Otolaryngology, Developmental and Integrative Biology, The University of Alabama at Birmingham, Birmingham Alabama

[3]Department of Biochemistry and Molecular Genetics, Developmental and Integrative Biology, The University of Alabama at Birmingham, Birmingham Alabama

[4]Department of Neurosurgery, Developmental and Integrative Biology, The University of Alabama at Birmingham, Birmingham Alabama

[5]Department of Cell, Developmental and Integrative Biology, The University of Alabama at Birmingham, Birmingham Alabama

[6]ChemoMetec, DK-3450 Allerod, Denmark

Abstract

Glioblastoma (GBM) is an aggressive malignancy with limited effectiveness of standard of care therapies including surgery, radiation, and temozolomide chemotherapy necessitating novel therapeutics. Unfortunately, GBMs also harbor several signaling alterations that protect them from traditional therapies that rely on apoptotic programmed cell death. Because almost all GBM tumors have dysregulated phosphoinositide signaling as part of that process, we hypothesized that peptide mimetics derived from the phospholipid binding domain of Myristoylated alanine-rich C-kinase substrate (MARCKS) could serve as a novel GBM therapeutic. Using molecularly classified patient-derived xenograft (PDX) lines, cultured in stem-cell conditions, we demonstrate that cell permeable MARCKS effector domain (ED) peptides potently target all GBM molecular classes while sparing normal human astrocytes. Cell death mechanistic testing revealed that these peptides produce rapid cytotoxicity in GBM that overcomes caspase inhibition. Moreover, we identify a GBM-selective cytolytic death mechanism involving plasma membrane targeting and intracellular calcium accumulation. Despite limited relative partitioning to the brain, tail vein peptide injection revealed tumor targeting in intracranially implanted GBM PDX. These results

Users may view, print, copy, and download text and data-mine the content in such documents, for the purposes of academic research, subject always to the full Conditions of use:http://www.nature.com/authors/editorial_policies/license.html#terms

Correspondence: Christopher D. Willey, MD, PhD, Department of Radiation Oncology, HSROC 2232C, 619 19th Street S, The University of Alabama at Birmingham, Birmingham, AL 35249, Phone: 205-934-5670, cwilley@uabmc.edu.

Supplementary information is available at Oncogene's website.

Author Manuscript Author Manuscript Author Manuscript Author Manuscript

Author Manuscript

indicate that MARCKS ED peptide therapeutics may overcome traditional GBM resistance mechanisms, supporting further development of similar agents.

Keywords

MARCKS; effector domain; glioblastoma; peptide therapeutic; phosphoinositides; patient-derived xenograft

Introduction

Glioblastoma (GBM; grade IV astrocytoma) is the most common primary adult brain malignancy and remains incurable, with a median survival around 15 months, despite the current standard of care of maximally safe surgical resection with adjuvant temozolomide (TMZ) and radiation therapy[1]. GBM therapies are needed that can overcome enhanced survival signaling, dysfunctional apoptotic signaling[2, 3], the presence of the blood-brain barrier, and high expression of efflux transporters present in GBM to become effectively cytotoxic and improve patient outcomes[4, 5]. The identification of appropriate drug targets and understanding therapeutic features in the context of these resistance mechanisms is both challenging and essential for developing new effective treatments for GBM.

GBM, like most cancers, have frequent dysregulations of phospholipid signaling that drive aggressive features including tumor growth, proliferation[6], invasion, radiation resistance[7, 8], immune evasion[9], and survival signaling[10, 11]. Phosphatidylinositol 3 kinase (PI3K) hyperactivation is considered a hallmark of cancer[12], and 90% of GBMs show dysregulated phosphatidylinositol 3 kinases (PI3K)/protein kinase B (AKT)/mammalian target of rapamycin (mTOR) signaling[10, 13], which can result from hyperactivation of receptor tyrosine kinases (RTKs), RAS[14] or mutations to phosphoinositide (PI) metabolizing enzymes themselves. Either hyperactivation of PI3K or frequent loss of phosphatase and tensin homolog (PTEN) can promote the phosphorylation of phosphatidylinositol 4,5-bisphosphate [Ptdlns(4,5)P_2] to produce phosphatidylinositol 3,4,5-trisphosphate [Ptdlns(3,4,5)P_3], leading to enhanced GBM aggressiveness and therapeutic resistance[8, 15]. Although the RTK/RAS/PI3K signaling pathway is a highly desirable target for GBM therapy[16, 17], attempts at targeting individual protein components of this pathway using small molecules or antibodies have shown little clinical success in GBM so far[18].

Myristoylated alanine-rich C-kinase substrate (MARCKS) effector domain (ED) (residues 151–175) is an electrostatically charged (+13) 25 amino acid region that is known to bind and sequester Ptdlns(4,5)P2, giving the MARCKS ED the potential to suppress this frequently dysregulated pathway. MARCKS ED is also known to bind phosphatidylserine (PS)[19], F-actin[20], calcium/calmodulin ($Ca^{2+/}$CaM)[20], serve as a phosphorylation substrate of PKC and ROCK kinases[21], function as a nuclear localization sequence[22–24], and most recently, been shown to bind polysialic acid[25]. MARCKS ED mimetics have been used in non-cancer systems to bind PS, acting as a curvature sensor [19] or as an anticoagulant by inhibiting fibrin formation[26]. Furthermore, ED mimetics have been shown to suppress growth, decrease AKT activation and [Ptdlns(3,4,5)P_3] accumulation in

Author Manuscript Author Manuscript Author Manuscript Author Manuscript

lung cancer[27], suppress growth and enhance tyrosine kinase inhibitor (TKI) sensitivity in renal cell carcinoma[28]. Our lab has previously used a cell penetrant version of MARCKS ED to suppress lung cancer growth and enhance its radiation sensitivity[29]. However, the effects of MARCKS ED mimetics on GBM are unknown.

In this study, we explore the therapeutic potential of MARCKS ED peptide for the treatment of GBM. As the efficacy of many GBM therapeutics is minimized by limited intracellular accumulation, we also assess the benefits of the covalent addition of a cell penetrant, trans-activator of transcription (TAT) sequence[30] linked to MARCKS ED peptide (TAT-ED or MED2). We explore the selective cytotoxic effects of MARCKS ED against a panel of molecularly subtyped GBM patient-derived xenograft (PDX) lines in comparison to normal human astrocytes (NHAs), and test its effects on caspase inhibition, addressing a common GBM resistance mechanism resulting from expression of inhibitor of apoptosis proteins (IAPs) [3] using a new image cytometry platform. Next, using a Cyanine 7 (CY7) labeled peptide we quantify the accumulation and localization of TAT-ED/MED2 into GBM *in vitro* and measure its BBB penetrance using tail-vein injections of TAT-ED/MED2 and assess GBM accumulation *in vivo*. Overall, we find MARCKS ED selectively binds to GBM cells *in vitro* with potent cytotoxic effects and although brain partitioning is low, the peptide can accumulate inside GBM PDX *in vivo* making it a potentially useful GBM targeting peptide with further development.

Results

MED2 dose-dependently decreases GBM cell viability at concentrations non-toxic to normal human astrocytes

The MARCKS ED is rich in poly-lysines producing some cell permeability. Indeed, MARCKS ED alone can prevent MARCKS phosphorylation at 50μM concentrations and reduce cell viability at 10–100μM concentrations in renal cell carcinoma[28] and lung cancer lines[27]. However, the addition of cell permeable sequences, such as HIV TAT, is expected to improve peptide penetration and potency. As such, we designed MARCKS ED peptides containing TAT sequences with or without near infrared labeling (Cy7) in patient-derived GBM models (Figure 1A). First, we compared effects on cell viability of MED2 vs a TAT control peptide (CTL2) (Figure 1A) against a cohort of molecularly classified GBM PDX (Figure 1B) including, classical (JX12, JX14, and JX39), mesenchymal (JX22 and JX59), and proneural (XD456 and X1441) subtypes. We found all tested GBM subtypes to be dose-dependently sensitive to MED2 in comparison to CTL2 (Figure 1C–E). Mesenchymal lines and the classical line JX14 had >50% reductions in viability seen at 10μM ($P<0.0001$), with classical lines JX12 and JX39 showing >50% reduction at 5μM ($p<0.0001$) (Figure 1C). Proneural lines were found to be most sensitive, with >50% reductions in viability at 2.5μM MED2 (Figure 1D & E). Fifty percent growth inhibition (GI50) concentrations of MED2 were 2.5μM for XD456 (R^2 =0.932) and 2.3μM for X1441 (R^2=0.913). To confirm that MED2 cytotoxicity was not simply due to higher lysine content as compared to CTL2, we also tested a pseudophosphorylated MED2 (MED2-PP) with substitution of aspartic acids for the serine residues which had no effect on viability (Supplementary Figure S1A and B). Conversely, 10μM MED2 showed no toxicity in NHAs;

Author Manuscript

Author Manuscript

Author Manuscript

Author Manuscript

instead, increases in viability at both 5μM ($p = 0.00317$) and 10μM MED2 ($p=0.0039$) were seen (Figure 1F). The GI50 for MED2 in NHAs was >40μM with additional NHAs sensitivity data available in Supplementary Figure S2. Comparisons of GBM sensitivity to an ED mimetic lacking TAT revealed 50μM was required for similar effects to 2.5μM of MED2 in both XD456 (Figure. 1G) and X1441 (Figure 1H), with GI50s of 53.2μM ($R^2=0.954$) and 32μM ($R^2=0.968$) respectively. Since MED2 was designed as a MARCKS mimetic, we expected that MED2 would maintain cytotoxicity regardless of MARCKS expression. To confirm this, we performed shRNA knockdown of MARCKS in XD456 and found that MED2 had equivalent cytotoxicity in control knockdown and MARCKS knockdown conditions (Supplementary Figure S1C and D).

MED2 induces rapid cytoplasmic retraction, membrane blebbing and is similarly cytotoxic to adherent or spheroid cultures

The timing of cell death offers clues into the cytotoxic mechanism[31], so we investigated the timing of MED2 effects using time-lapse imaging of XD456. Noticeable morphological effects and signs of cellular injury began within 1 hour of MED2 treatment, indicated by retraction of cellular processes that continued until the majority of cells had contracted into clusters by 6 hours (Figure 2A). Using a membrane impermeable nuclear dye (SYTOX), we measured plasma and nuclear membrane permeabilization and found uptake within 1 hour of MED2 treatment (Figure 2B). A time-lapse video of MED2 cytotoxicity in XD456 is available in Supplementary Video S1. Next, we investigated if MED2 treatment was relatively modulated in adherent cells as compared to non-adherent neurospheres as cellular attachment is associated with cancer stemness, and a wide array of intracellular signaling consequences that may affect sensitivity to therapeutic agents[32]. Testing in multiple PDX subtypes showed equally effective inhibition of viability in adherent or suspension cells ($p>0.05$) (Supplementary Figure S2A). Closer examination of MED2 cytotoxic effects revealed in addition to the contraction of cytoplasmic processes, cells also developed a rough blebbed appearance to the plasma membrane (Figure 2C, white arrows) by 5 hours, an indication of plasma membrane stress [33]. These findings reveal MED2 cytotoxicity is rapid, with similar efficacy in GBM in both adherent and non-adherent neurosphere conditions.

To understand these cytotoxic effects and associated alterations, we performed an apoptosis assay using the Xcyto10 image cytometer. In comparison to CTL2, MED2 treatment caused cells to concurrently co-stain for Annexin-V and SYTOX at 5 hours with no meaningful changes in Annexin-V^{positive}/SYTOX^{negative} or Annexin-V^{negative}/SYTOX^{positive} populations observed (Figure 2D). Specifically, we did not detect an increase in Annexin-V^{positive}/SYTOX^{negative} cells, which is indicative of early apoptosis[34]. Xcyto10 image cytometry allows direct comparison of cells selected from images (Figure 2E, circled in pink and numbered) to their corresponding data points (Figure 2D, numbered pink crosses). We noted slight increases of Annexin-V intensity in the Annexin-V^{negative}/SYTOX^{negative} population (rightward shift of MED2 compared to CTL2), which was found to be from formation of Annexin-V positive blebs (green arrows) and differs from a fully Annexin-V^{positive} cell (yellow arrow) (Figure 2F). Closer examination shows the distinct differences in an Annexin-V^{positive} cell, with uniform Annexin-V binding (Figure 2G), to Annexin-V

Author Manuscript Author Manuscript Author Manuscript Author Manuscript

blebbing (Figure 2H). Bleb diameter was approximately 2–5μm in diameter and a consistent finding with MED2 treatment of GBM PDX lines. Additional information on Xcyto10 fluorescent multiplexing is found in Supplementary Figures S3–S6. Assessing the cleavage fragments of poly ADP-ribose polymerase (PARP1) can also give insight into the form of cell death since it is the substrate of several distinct proteolytic proteins that play roles in various forms of cell death[35]. Loss of PARP1's 122kD band with the formation of an 89 kD fragment is indicative of apoptosis, and a caspase mediated cleavage[35]. However, we instead found a loss of both 122kD and 89kD bands with the formation of an approximately 72 kD band. Since membrane blebbing is a response to plasmalemmal injury that can occur from calcium-independent or dependent mechanisms and commonly associated with apoptosis[33], we investigated if MED2's cytotoxic effects were dependent on pro-apoptotic caspases.

MED2's cytotoxicity is resistant to caspase inhibition

To examine the possibility that MED2 cytotoxicity does not require a caspase-dependent apoptotic mechanism[36], we pretreated GBM cells with caspase inhibitors and either MED2 or cisplatin, a well-studied inducer of apoptosis[37]. Both QVD-OPh and Z-VAD-FMK have potent anti-apoptotic effects through broad inhibition of caspases at low micromolar concentrations[38]. Cisplatin's cytotoxic effects are slower than MED2's, so testing at 24 hours showed a cisplatin-induced increase of Annexin-V^{positive} cells in X1441 that is blocked entirely with pretreatment with QVD-OPh (Figure 3A). Activation of caspase-3 and caspase-7 is also blocked by this high concentration of QVD-OPh or Z-VAD-FMK (Figure 3B). However, similar caspase inhibitor concentrations showed no protection against MED2 cytotoxicity up to 9 hours (Figure 3C). MED2 treatment increased caspase 3/7 activation ($P<0.001$) compared with CTL2, but equivalent doses of QVD-OPh or ZVAD-FMK only inhibited caspase activation by 25% or 65% respectively. Doubling the QVD-OPh achieved a 50% reduction in caspase activation (Figure 3D), with no effect on cytotoxicity, while higher ZVAD-FMK doses failed to achieve further caspase inhibition. Testing of these high QVD-OPh concentrations in multiple GBM subtypes showed no impact on MED2's cytotoxicity (Figure 3E). MED2-induced GBM cell death is resistant to the effects of caspase inhibition; therefore, we investigated if dysregulations in calcium are possibly mediating MED2 cytotoxic effects.

MED2 triggers sustained increases in intracellular calcium

Calcium overload can trigger retraction of cytoplasmic processes, promote membrane blebbing and activate caspase-independent cell death[39]. Using a Fluo-4 calcium indicator and serial imaging, we found that Fluo-4 intensity increased within minutes of MED2 treatment of XD456 and continued to increase over two hours (Figure 4A). Direct comparison of MED2 effects in GBM vs. NHAs found that XD456 and X1441 had substantial increases in Fluo-4 and SYTOX intensity over CTL2 treated cells, whereas NHAs showed considerably smaller increases in Fluo-4 and SYTOX intensity (Figure 4B). This indicates that MED2 preferentially increases intracellular calcium in GBM as compared to NHAs and this correlates with cytotoxicity.

Author Manuscript Author Manuscript Author Manuscript Author Manuscript

We attempted to block MED2 cytotoxicity through chelation of free calcium using BAPTA-AM[40]. Pretreatment with BAPTA showed no protective effects in multiple GBM subtypes at low concentrations and decreased viability at higher concentration (Figure 4C). Both time-course (Figure 4D) and endpoint experiments (Figure 4E) revealed that high dose BAPTA pretreatment could significantly suppress MED2 Fluo-4 fluorescence in GBM ($p<0.0001$) and NHAs($p<0.001$). However, BAPTA demonstrated no protective effects, instead showing greater overall cytotoxicity in GBM ($p<0.0001$), but not in NHAs ($p=0.849$) (Figure 4F). We suspected that the differential efficacy of MED2 between NHA and GBM cells might be due to differences in peptide accumulation.

MED2 shows preferential binding to, and accumulation in GBM over NHAs *in vitro*

We compared the accumulation of MED2-CY7 in XD456, X1441 and NHAs and found that within 10 minutes, GBM lines demonstrated numerous bright MED2 accumulations at the plasma membrane (blue arrows) more frequently than NHAs (Figure 5A), with differences most apparent 30 minutes to 1-hour post-treatment (Figure 5B). MED2 accumulations varied in number, size, and location per cell but remained distinct in appearance (Figure 5C). Fixation and visualization of these cells after 1.5 hours of treatment showed greater MED2 fluorescence and nuclear accumulation in GBM relative to NHAs (Figure 5D). Quantification of MED2-CY7 fluorescence per cell revealed XD456 and X1441 acquired double the mean fluorescence of NHAs by 1.5-hours (11.2 ± 0.39, 11.7 ± 0.75 & $5.9 \pm 0.27 \times 10^6$ respectively, Mean ± SEM) (Figure 5E). Longer (9-hour) incubations with 2.5μM MED2-CY7 similarly show GBM with greater increases of MED2 accumulation, and cytotoxicity, compared with NHAs. Although NHAs accumulated substantial amounts of MED2-CY7 (Figure 5F), it remained cytoplasmic (Supplementary Fig. S7). Using 1μM MED2-CY7, a dose selected to limit cytotoxicity, we found NHAs and XD456 can accumulate similar levels of cytoplasmic MED2 at longer incubations, but not nuclear accumulation ($p<0.0001$) (Figure 5G and Supplementary Figure S7B). These findings reveal that MED2 *in vitro* will preferentially bind and accumulate inside GBM over NHAs. Control peptide with Cy7 labeling (CTL2-CY7) did not bind and accumulate on GBM cells nor did it produce cytotoxicity suggesting that Cy7 labeling is not responsible for the MED2-CY7 cytotoxicity (Supplementary Figure S8).

MED2 crosses the blood-brain barrier and concentrates in the periventricular brain region in orthotopic tumors

To assess MED2's ability to cross the blood-brain barrier (BBB) and identify if preferential binding to GBM continues *in vivo*, we assessed brain accumulation of 5 or 10 nanomoles MED2-CY7, 3 hours after tail-vein injection into tumor-naïve nude mice. Assessment of MED2-CY7 biological-distribution in the major organs revealed the greatest intensity per mg tissue was in the kidney, liver, small and large intestines, respectively with only a small percentage of total peptide reaching the brain (See Figure 6A). Nevertheless, we did identify dose-dependent increases of MED2-CY7 fluorescence in periventricular regions of the brain (Figure 6B), with a greater than threefold ($p=0.026$) increase in fluorescence with the higher dose ($n=3$) (Figure 6C). Despite the limited brain partitioning, we did explore whether MED2-CY7 could concentrate within GBM PDX orthotopically implanted into mice. This revealed substantial increases of MED2-CY7 fluorescence (red high, blue low) in tumor-

Author Manuscript Author Manuscript Author Manuscript Author Manuscript

burdened regions of the brain as compared to normal brain (Figure 6D), suggesting MED2 will cross the BBB and preferentially accumulate in GBM as compared to normal brain.

Discussion

GBM is a heterogeneous disease demonstrating multiple potential alterations in survival and cell death pathways[4, 10] promoting robust therapeutic resistance. Additionally, high expression of drug efflux transporters in GBM[41] and the presence of the BBB limit the intracellular accumulation of many chemotherapies[5] restricting their effectiveness[42]. Consideration of these challenges early in preclinical investigations can greatly enhance the translational utility of the study, so we assessed MED2's potential as a GBM therapy in the context of potential resistance mechanisms.

Screening of proneural, classical and mesenchymal subtypes confirmed MED2 has substantial dose-dependent cytotoxicity in multiple GBM subtypes but not NHAs; The proneural subtype was most sensitive, with GI50s around 2.5μM, while classical and mesenchymal subtypes GI50 ranged from 5μM – 10μM. Although differences were modest, the most sensitive lines were TP53 deleted/null (XD456, JX12, and JX39) and PTEN wild-type (WT), while the least sensitive was TP53 WT (JX59, JX22, JX14) and/or were PTEN deleted (JX59 & JX14). We did not find any relationship with EGFR status. Since MARCKS protein expression has been linked to adhesion and invasive properties of EGFRvIII,[43] it is possible that MARCKS-ED mimetics may impact additional aspects of glioma biology depending on the genetic context of the tumor cell.

A hallmark of cancer is an evasion of apoptosis[2], a type-1 cell death with features such as cytoplasmic shrinkage, chromatin condensation, plasma membrane blebbing and formation of apoptotic bodies, typically mediated by caspases[36]. Apoptosis classically maintains plasma membrane integrity throughout the cell death process resulting in increases of Annexin-$V^{positive}$ (PS externalization) /$SYTOX^{negative}$ (maintained plasma membrane integrity) cells before increases in Annexin-$V^{positive}$/$SYTOX^{positive}$ (lost plasma and nuclear membrane integrity)[36], as observed with cisplatin treatment of X1441. We found MED2 resulted in cytoplasmic contraction and membrane blebbing, but direct increases in Annexin-$V^{positive}$ /$SYTOX^{positive}$. This concurrent staining along with the rapid onset of effects, and the findings from the PARP1 Western blot that did not show the formation of an 89kD fragment typical of apoptosis[35] suggested the MED2 cytotoxic mechanism likely differs from caspase-mediated apoptosis[34].

One mechanism GBM has to prevent apoptosis is through inhibition of caspases by upregulating inhibitor of apoptosis protein (IAP) expression[3, 4], creating a clinical need for cytotoxic therapies not dependent on caspases. We determined MED2 cytotoxicity is resistant to caspase inhibition and likely to overexpression of IAP's. Difficulties in fully inhibiting MED2 caspase activation, measured using a fluorescent indicator of DEVD sequence cleavage, at extremely high inhibitor concentrations suggests MED2 alternatively activates proteolytic proteins or alters their ability to be inhibited. Calcium's role in inducing membrane blebbing[33], activation of alternative proteolytic proteins like calpain[44], and functioning in programmed cell death[45], prompted us to investigate MED2 effects on

Author Manuscript Author Manuscript Author Manuscript Author Manuscript

intracellular calcium, where MED2 was found to promote greater sustained increases in intracellular calcium in GBM than in NHAs. This finding, along with the failure of calcium chelation to prevent MED2 cytotoxicity, the rapid SYTOX uptake by apoptosis assay, and the differential binding pattern seen with fluorescent imaging, leads us to propose that MED2 cytotoxicity results from its substantial calcium influx through an unknown mechanism that results in a loss of membrane integrity. MED2 cytotoxicity may occur from dysregulation of membrane channels (i.e. calcium) or direct membrane permeabilization similar to classes of anti-cancer cytotoxic peptides[46]. Benefits of membrane permeabilizing therapies include the release of pro-inflammatory mediators[47] and potential tumor antigens, making it an immunogenic cell death with potential value as an adjuvant therapy along with immunotherapies.

Substantial plasma membrane differences exist between cancer and normal cells[9, 46], and the pattern of membrane MED2-CY7 accumulations on GBM suggest MED2 is binding currently unknown plasma membrane features abundantly found in GBM. Indeed, a very recent report identifies enhanced polyunsaturated fatty acid synthesis in GBM stem cells, which are cells similar to those used in our study. The alterations they found in membrane phospholipid composition were key determinants of GBM phenotype and treatment sensitivity[48]. In addition, MARCKS ED peptide has also been shown to effectively bind cell surface polysialic acid through a combination of electrostatic and phenylalanine interactions. A fluorescently tagged MARCKS-ED peptide detected polysialic acid, particularly in the spinal trigeminal nucleus and dorsal vagal complex in rat brainstem tissue sections.[25] Our work with the pseudo-phosphorylated version of the peptide (MED2-PP) suggests that the serine residues are key for the cytotoxicity of the peptide likely through altered interactions. As such, identification of MED2-specific membrane-binding partners may prove useful for future targeted GBM therapeutics and is of significant ongoing interest. Exploratory studies of downstream signaling suggests that the MARCKS-ED peptide downregulates several non-receptor tyrosine kinases that promotes altered gene expression (Supplementary Figure S9). Future studies are needed to elucidate the connection between cell surface binding of the peptide and these downstream events.

In vivo studies showed only a small percentage of MED2-CY7 partitioning in the brain which precluded *in vivo* survival studies. Even though MED2-CY7 demonstrated preferential intracranial tumor accumulation with only minimal periventricular signal seen in tumor naïve mice, the current formulation of this peptide is unlikely to effectively penetrate the brain through systemic delivery. Additional studies are needed to enhance delivery of therapeutic peptides to the brain[42] in order to demonstrate *in vivo* efficacy.

In conclusion, few current therapies trigger potent cytotoxic effects against GBM and identifying therapies that accumulate well in GBM, remain cytotoxic despite deficiencies in cell death pathways, and that generate immunogenic modes of cell death[47], provide the best opportunities to improve patient outcomes. This study demonstrates useful techniques in studying how a cell penetrating peptide of MARCKS ED possesses rapid, potent and selective cytolytic features against GBM that may one day be useful for enhancing patient outcomes.

Author Manuscript

Materials and Methods

An extended methods section is available in Supplementary Materials available online.

PDX culturing.

All PDX tissue was acquired through the University of Alabama at Birmingham Brain Tumor Animal Model core, and the animal research was approved by the local ethics committee (IACUC-10159). PDX were generated and propagated as previously described[49, 50]. PDX molecular subtypes were determined from Verhaak gene signature[51] and mutational status of 40 select genes identified by Roche 454 Jr sequencing. PDX were maintained in neurosphere media described above with NHAs maintained in standard media. Accutase (Corning) was used for cell disassociation and Geltrex (GIBCO) aided cell attachment. STR profiling is done routinely by the Brain Tumor Animal Model Core and the Willey laboratory.

MARCKS peptides.

MED2, CTL2, MED2-CY7, and CTL2-CY7 were created similar to the previously described methods used to generate MED1[29] and reconstituted in PBS. A detailed protocol for peptide synthesis of ED mimetics can be found in the Supplemental Methods.

Cell viability.

1×10^4 live cells, counted using Trypan blue staining, were plated into a black-walled 96 well plate (PerkinElmer) in 4X replicates with 90μL media. 10μL of 10X concentrated peptide diluted in media was added 2 hours post plating and plates were assayed after 72 hours using CellTiter-Glo ATP luminescence (Promega) protocol.

Xcyto10 apoptosis assay.

2.5×10^5 cells plated in 12 well plates overnight, were treated at indicated doses for indicated time points, before collecting media, lifting cells and staining at RT for 30min in 250μL Annexin-V, SYTOX, caspase staining solution [per 500μL 1X Annexin-V binding buffer (Thermo), add 1 drop of Annexin-V AlexaFluor 647 ready-flow (Invitrogen), 1μL SYTOX orange (Invitrogen), 1 drop cell-event green caspase 3/7 dye (Invitrogen)]. Cells briefly mixed before loading 45μL into Xcyto 2-Chamber slide (ChemoMetec) and imaging on Xcyto10 (ChemoMetec) at 4X magnification with compensation of channels predetermined. Plots generated in XcytoView (ChemoMetec). See Supplementary Methods and Figures S3–S6.

Adherent cell imaging: MED2 localization and quantification.

1×10^5 cells adhered to glass coverslips (Corning), treated with MED2-CY7 were and imaged with EVOS FL (AMG) at 10X magnification for live cell imaging. MED2-CY7 localization accomplished in 4% Paraformaldehyde-fixed, 0.1% Triton-X permeabilized cells co-stained with 1:1000 BlueMask-1(ChemoMetec) and DAPI (2μg/mL), mounted on Xcyto 2-sample slides (ChemoMetec) and imaged with Xcyto10 at 20X magnification for intracellular quantification. Mean fluorescent intensity of nuclear and cytoplasmic

Author Manuscript Author Manuscript Author Manuscript Author Manuscript

compartments determined using XcytoView. CellInsight CX7 (ThermoFisher) SYTOX intensity quantification acquired using a heated chamber with CO2 and imaged in 5-minute intervals at 20X magnification using Hoechst and SYTOX orange channels.

Calcium imaging.

1×10^5 cells were attached in 24 well plates. Media replaced with 500μL of 1X Fluo-4 direct calcium assay buffer supplemented with 5mM probenecid per manufacturer (Invitrogen) at 37C for 1.5 hours before addition of SYTOX and peptide. Live cell images acquired on AMG EVOS FL at 10X magnification using GFP and RFP channels. Fluor-4 and SYTOX intensity were measured in suspension cells at 4X magnification on Xcyto10, with fluorescence compensation, using 2-chamber slides. Time-lapse mean fluorescence intensity in live cells was acquired in 3-minute intervals of 4 individual fields of view at 20X magnification using CellInsight CY7 and GFP channels.

In vivo MED2-CY7 biodistribution.

All animal studies were UAB Occupational Health & Safety approved (Project #14–124) and carried out in accordance with the policies and guidelines set by the Institutional Animal Care and Use Committee (IACUC Animal Project Number #10159). Briefly[49], 6-week-old female athymic nude mice (Charles River; Hartford, CT) were stereotactically injected with 5×10^5 X1016 cells into the caudate putamen 1 week before biodistribution studies. Animals were sorted by bioluminescence imaging to have similar tumor burden between groups and then the two groups were randomized to the two dose levels but the investigators were not blinded. MED2-CY7 diluted in 100 μL of normal saline was injected via tail vein, and mice sacrificed 3 hours later. Major organs were collected and weighed before imaging on Pearl Imaging System (LI-COR Biosciences) at 700nm channel using uniform Z-plane thickness similar to previous work.[52] The brain was formalin fixed overnight before sectioning, gross fluorescent imaging, and paraffin embedding and mounting. Consecutive sections were H&E stained or fluorescence intensity determined using an Odyssey CLx (LI-COR Biosciences) at 700nm channel. Fluorescent intensity per mg of tissue was calculated in excel and graphed using Prism. For comparisons, the color scale was kept uniform for each group of images.

Statistical analysis, IC50 calculations, data reproducibility.

Sample sizes were estimated based off of prior related studies.[29, 52, 53] Statistical analyses were calculated in Prism 8.0 (GraphPad) with p values of < 0.05 considered statistically significant. GI50s interpolated from a standard curve generated in Prism. All experiments repeated at least two times. * $p<0.05$, ** $p<0.01$, *** $p<0.001$, **** $p<0.0001$.

Data availability.

Data presented in this manuscript are available from the corresponding author upon request.

Supplementary Material

Refer to Web version on PubMed Central for supplementary material.

Author Manuscript
Author Manuscript
Author Manuscript
Author Manuscript

Acknowledgments

A special thanks to Neil A. Durso, Ph.D. from ThermoFisher for assistance with time-lapse and calcium imaging using CellInsight Cx7 instrument. ChemoMetec loaned us the Xcyto10 image cytometer for initial work and provided microscope slides, BlueMask-1and DAPI reagents but no financial compensation. We would also like to acknowledge the UAB Nanostring Laboratory in the Department of Radiation Oncology, directed by Eddy S. Yang, MD, PhD and managed by Debbie Della Manna, as well as the UAB Kinome Core for the molecular analyses services performed in the supplementary data.

Competing Interests

This work was supported by funding from the National Institutes of Health (the UAB MSTP training grant: T32GM008361 and the UAB Training Program in Brain Tumor Biology: T32NS048039), the American Cancer Society RSG-14-071-01-TBG, the UAB Physician Scientist Training Program Medical Student Summer Research Training Program, and an intramural research grant from the UAB Department of Radiation Oncology. Rune T. Pedersen is an employee at ChemoMetec and assisted in the use of Xcyto10, aided in Xcyto10 data analysis, and reviewed the manuscript. Unrelated to this work, but for full disclosure, Dr. Willey is a part time consultant with LifeNet Health and Varian Medical Systems.

References:

1. Stupp R, Mason WP, van den Bent MJ, Weller M, Fisher B, Taphoorn MJ et al. Radiotherapy plus concomitant and adjuvant temozolomide for glioblastoma. The New England journal of medicine 2005; 352: 987–996. [PubMed: 15758009]
2. Fulda S Tumor resistance to apoptosis. Int J Cancer 2009; 124: 511–515. [PubMed: 19003982]
3. Tchoghandjian A, Souberan A, Tabouret E, Colin C, Denicolai E, Jiguet-Jiglaire C et al. Inhibitor of apoptosis protein expression in glioblastomas and their in vitro and in vivo targeting by SMAC mimetic GDC-0152. Cell Death Dis 2016; 7: e2325. [PubMed: 27490930]
4. Krakstad C, Chekenya M. Survival signalling and apoptosis resistance in glioblastomas: opportunities for targeted therapeutics. Mol Cancer 2010; 9: 135. [PubMed: 20515495]
5. Wijaya J, Fukuda Y, Schuetz JD. Obstacles to Brain Tumor Therapy: Key ABC Transporters. International journal of molecular sciences 2017; 18.
6. Vadlakonda L, Pasupuleti M, Pallu R. Role of PI3K-AKT-mTOR and Wnt Signaling Pathways in Transition of G1-S Phase of Cell Cycle in Cancer Cells. Frontiers in oncology 2013; 3: 85. [PubMed: 23596569]
7. Chang L, Graham PH, Hao J, Ni J, Bucci J, Cozzi PJ et al. Acquisition of epithelial-mesenchymal transition and cancer stem cell phenotypes is associated with activation of the PI3K/Akt/mTOR pathway in prostate cancer radioresistance. Cell Death Dis 2013; 4: e875. [PubMed: 24157869]
8. Toulany M, Rodemann HP. Phosphatidylinositol 3-kinase/Akt signaling as a key mediator of tumor cell responsiveness to radiation. Seminars in cancer biology 2015; 35: 180–190. [PubMed: 26192967]
9. Birge RB, Boeltz S, Kumar S, Carlson J, Wanderley J, Calianese D et al. Phosphatidylserine is a global immunosuppressive signal in efferocytosis, infectious disease, and cancer. Cell Death Differ 2016; 23: 962–978. [PubMed: 26915293]
10. Cancer Genome Atlas Research N. Comprehensive genomic characterization defines human glioblastoma genes and core pathways. Nature (Research Support, N.I.H., Extramural) 2008; 455: 1061–1068.
11. Hanahan D, Weinberg RA. Hallmarks of cancer: the next generation. Cell 2011; 144: 646–674. [PubMed: 21376230]
12. Fruman DA, Chiu H, Hopkins BD, Bagrodia S, Cantley LC, Abraham RT. The PI3K Pathway in Human Disease. Cell 2017; 170: 605–635. [PubMed: 28802037]
13. Langhans J, Schneele L, Trenkler N, von Bandemer H, Nonnenmacher L, Karpel-Massler G et al. The effects of PI3K-mediated signalling on glioblastoma cell behaviour. Oncogenesis 2017; 6: 398. [PubMed: 29184057]
14. Castellano E, Downward J. RAS Interaction with PI3K: More Than Just Another Effector Pathway. Genes & cancer 2011; 2: 261–274. [PubMed: 21779497]

Author Manuscript Author Manuscript Author Manuscript Author Manuscript

15. Denley A, Gymnopoulos M, Kang S, Mitchell C, Vogt PK. Requirement of phosphatidylinositol(3,4,5)trisphosphate in phosphatidylinositol 3-kinase-induced oncogenic transformation. Mol Cancer Res 2009; 7: 1132–1138. [PubMed: 19584261]
16. Nichol D, Mellinghoff IK. PI3K pathway inhibition in GBM-is there a signal? Neuro Oncol 2015; 17: 1183–1184. [PubMed: 26170259]
17. Li X, Wu C, Chen N, Gu H, Yen A, Cao L et al. PI3K/Akt/mTOR signaling pathway and targeted therapy for glioblastoma. Oncotarget 2016.
18. Wen PY, Lee EQ, Reardon DA, Ligon KL, Alfred Yung WK. Current clinical development of PI3K pathway inhibitors in glioblastoma. Neuro Oncol 2012; 14: 819–829. [PubMed: 22619466]
19. Morton LA, Yang H, Saludes JP, Fiorini Z, Beninson L, Chapman ER et al. MARCKS-ED peptide as a curvature and lipid sensor. ACS chemical biology 2013; 8: 218–225. [PubMed: 23075500]
20. Arbuzova A, Schmitz AA, Vergeres G. Cross-talk unfolded: MARCKS proteins. Biochem J 2002; 362: 1–12. [PubMed: 11829734]
21. Tanabe A, Kamisuki Y, Hidaka H, Suzuki M, Negishi M, Takuwa Y. PKC phosphorylates MARCKS Ser159 not only directly but also through RhoA/ROCK. Biochem Biophys Res Commun 2006; 345: 156–161. [PubMed: 16677610]
22. Brudvig JJ, Weimer JM. X MARCKS the spot: myristoylated alanine-rich C kinase substrate in neuronal function and disease. Front Cell Neurosci 2015; 9: 407. [PubMed: 26528135]
23. Fong LWR, Yang DC, Chen CH. Myristoylated alanine-rich C kinase substrate (MARCKS): a multirole signaling protein in cancers. Cancer Metastasis Rev 2017.
24. Rohrbach TD, Shah N, Jackson WP, Feeney EV, Scanlon S, Gish R et al. The Effector Domain of MARCKS Is a Nuclear Localization Signal that Regulates Cellular PIP2 Levels and Nuclear PIP2 Localization. PLoS One 2015; 10: e0140870. [PubMed: 26470026]
25. Iqbal S, Walsh TR, Rodger A, Packer NH. Interaction between Polysialic acid and MARCKS-ED peptide at the molecular level. ACS Chem Neurosci 2020.
26. Kastelowitz N, Tamura R, Onasoga A, Stalker TJ, White OR, Brown PN et al. Peptides derived from MARCKS block coagulation complex assembly on phosphatidylserine. Scientific reports 2017; 7: 4275. [PubMed: 28655899]
27. Chen CH, Statt S, Chiu CL, Thai P, Arif M, Adler KB et al. Targeting myristoylated alanine-rich C kinase substrate phosphorylation site domain in lung cancer. Mechanisms and therapeutic implications. American journal of respiratory and critical care medicine 2014; 190: 1127–1138. [PubMed: 25318062]
28. Chen CH, Fong LWR, Yu E, Wu R, Trott JF, Weiss RH. Upregulation of MARCKS in kidney cancer and its potential as a therapeutic target. Oncogene 2017; 36: 3588–3598. [PubMed: 28166200]
29. Rohrbach TD, Jones RB, Hicks PH, Weaver AN, Cooper TS, Eustace NJ et al. MARCKS phosphorylation is modulated by a peptide mimetic of MARCKS effector domain leading to increased radiation sensitivity in lung cancer cell lines. Oncology letters 2017; 13: 1216–1222. [PubMed: 28454237]
30. Dinca A, Chien WM, Chin MT. Intracellular Delivery of Proteins with Cell-Penetrating Peptides for Therapeutic Uses in Human Disease. International journal of molecular sciences 2016; 17: 263. [PubMed: 26907261]
31. Panzarini E, Inguscio V, Dini L. Timing the multiple cell death pathways initiated by Rose Bengal acetate photodynamic therapy. Cell Death Dis 2011; 2: e169. [PubMed: 21654827]
32. Seguin L, Desgrosellier JS, Weis SM, Cheresh DA. Integrins and cancer: regulators of cancer stemness, metastasis, and drug resistance. Trends Cell Biol 2015; 25: 234–240. [PubMed: 25572304]
33. Babiychuk EB, Monastyrskaya K, Potez S, Draeger A. Blebbing confers resistance against cell lysis. Cell Death Differ 2011; 18: 80–89. [PubMed: 20596076]
34. Wlodkowic D, Telford W, Skommer J, Darzynkiewicz Z. Apoptosis and beyond: cytometry in studies of programmed cell death. Methods Cell Biol 2011; 103: 55–98. [PubMed: 21722800]
35. Chaitanya GV, Steven AJ, Babu PP. PARP-1 cleavage fragments: signatures of cell-death proteases in neurodegeneration. Cell Commun Signal 2010; 8: 31. [PubMed: 21176168]

36. Elmore S Apoptosis: a review of programmed cell death. Toxicol Pathol 2007; 35: 495–516. [PubMed: 17562483]

37. Dasari S, Tchounwou PB. Cisplatin in cancer therapy: molecular mechanisms of action. Eur J Pharmacol 2014; 740: 364–378. [PubMed: 25058905]

38. Keoni CL, Brown TL. Inhibition of Apoptosis and Efficacy of Pan Caspase Inhibitor, Q-VD-OPh, in Models of Human Disease. J Cell Death 2015; 8: 1–7. [PubMed: 25922583]

39. Zhivotovsky B, Orrenius S. Calcium and cell death mechanisms: a perspective from the cell death community. Cell Calcium 2011; 50: 211–221. [PubMed: 21459443]

40. Collatz MB, Rudel R, Brinkmeier H. Intracellular calcium chelator BAPTA protects cells against toxic calcium overload but also alters physiological calcium responses. Cell Calcium 1997; 21: 453–459. [PubMed: 9223681]

41. Haar CP, Hebbar P, Wallace GCt, Das A, Vandergrift WA 3rd, Smith JA et al. Drug resistance in glioblastoma: a mini review. Neurochem Res 2012; 37: 1192–1200. [PubMed: 22228201]

42. Groothuis DR. The blood-brain and blood-tumor barriers: a review of strategies for increasing drug delivery. Neuro Oncol 2000; 2: 45–59. [PubMed: 11302254]

43. Micallef J, Taccone M, Mukherjee J, Croul S, Busby J, Moran MF et al. Epidermal growth factor receptor variant III-induced glioma invasion is mediated through myristoylated alanine-rich protein kinase C substrate overexpression. Cancer Res (Research Support, Non-U.S. Gov't) 2009; 69: 7548–7556.

44. Johnson DE. Noncaspase proteases in apoptosis. Leukemia 2000; 14: 1695–1703. [PubMed: 10995018]

45. Galluzzi L, Vitale I, Aaronson SA, Abrams JM, Adam D, Agostinis P et al. Molecular mechanisms of cell death: recommendations of the Nomenclature Committee on Cell Death 2018. Cell Death Differ 2018.

46. Boohaker RJ, Lee MW, Vishnubhotla P, Perez JM, Khaled AR. The use of therapeutic peptides to target and to kill cancer cells. Current medicinal chemistry 2012; 19: 3794–3804. [PubMed: 22725698]

47. Kepp O, Tesniere A, Schlemmer F, Michaud M, Senovilla L, Zitvogel L et al. Immunogenic cell death modalities and their impact on cancer treatment. Apoptosis 2009; 14: 364–375. [PubMed: 19145485]

48. Gimple RC, Kidwell RL, Kim LJY, Sun T, Gromovsky AD, Wu Q et al. Glioma Stem Cell-Specific Superenhancer Promotes Polyunsaturated Fatty-Acid Synthesis to Support EGFR Signaling. Cancer Discov 2019; 9: 1248–1267. [PubMed: 31201181]

49. Willey CD, Gilbert AN, Anderson JC, Gillespie GY. Patient-Derived Xenografts as a Model System for Radiation Research. Semin Radiat Oncol 2015; 25: 273–280. [PubMed: 26384275]

50. Sarkaria JN, Carlson BL, Schroeder MA, Grogan P, Brown PD, Giannini C et al. Use of an orthotopic xenograft model for assessing the effect of epidermal growth factor receptor amplification on glioblastoma radiation response. Clin Cancer Res 2006; 12: 2264–2271. [PubMed: 16609043]

51. Verhaak RG, Hoadley KA, Purdom E, Wang V, Qi Y, Wilkerson MD et al. Integrated genomic analysis identifies clinically relevant subtypes of glioblastoma characterized by abnormalities in PDGFRA, IDH1, EGFR, and NF1. Cancer Cell 2010; 17: 98–110. [PubMed: 20129251]

52. de Boer E, Samuel S, French DN, Warram JM, Schoeb TR, Rosenthal EL et al. Biodistribution Study of Intravenously Injected Cetuximab-IRDye700DX in Cynomolgus Macaques. Mol Imaging Biol 2016; 18: 232–242. [PubMed: 26335283]

53. Jarboe JS, Anderson JC, Duarte CW, Mehta T, Nowsheen S, Hicks PH et al. MARCKS Regulates Growth, Radiation Sensitivity and Is a Novel Prognostic Factor for Glioma. Clinical Cancer Research 2012; doi: 10.1158/1078-0432.CCR-11-3091.

Author Manuscript

Author Manuscript

Author Manuscript

Author Manuscript

Author Manuscript
Author Manuscript
Author Manuscript
Author Manuscript

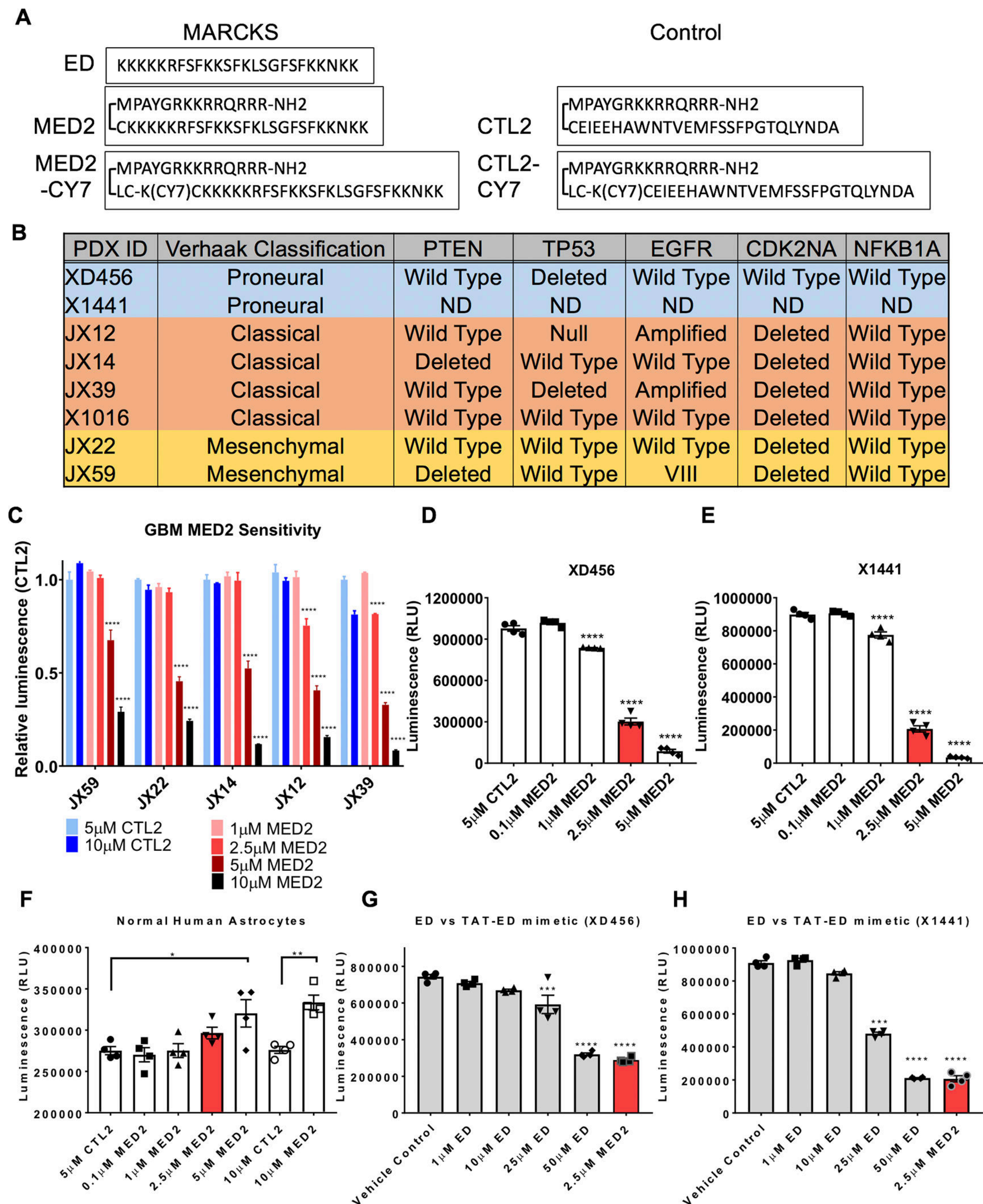

PDX ID	Verhaak Classification	PTEN	TP53	EGFR	CDK2NA	NFKB1A
XD456	Proneural	Wild Type	Deleted	Wild Type	Wild Type	Wild Type
X1441	Proneural	ND	ND	ND	ND	ND
JX12	Classical	Wild Type	Null	Amplified	Deleted	Wild Type
JX14	Classical	Deleted	Wild Type	Wild Type	Deleted	Wild Type
JX39	Classical	Wild Type	Deleted	Amplified	Deleted	Wild Type
X1016	Classical	Wild Type	Wild Type	Wild Type	Deleted	Wild Type
JX22	Mesenchymal	Wild Type	Wild Type	Wild Type	Deleted	Wild Type
JX59	Mesenchymal	Deleted	Wild Type	VIII	Deleted	Wild Type

Figure 1.

MARCKS ED mimetic cytotoxicity in GBM. **(A)** The sequence of ED without TAT, and MED2 with a covalent 3-maleimidopropionic acid (MPA) linkage between TAT and ED. MED2-CY7 incorporates a fluorescent cyanine CY7 dye. **(B)** PDX lines with Verhaak molecular subtypes and mutational status of select genes previously determined. ND=Not determined. **(C)** The relative viability of MED2 treated PDX. 1–5μM MED2 mean luminescence (RLU) normalized to 5μM CTL2, 10μM MED2 luminescence normalized to 10μM CTL2. **(D-H)** Cell viability effects of MED2/CTL2 treatment in **(D)** XD456, **(E)**

X1441, and **(F)** NHAs. Cell viability effects of ED lacking TAT, compared to 2.5μM MED2 (red colored bar), in **(G)** XD456 and **(H)** X1441. (C-H) Relative-Mean/Mean ± SEM. (C) 2-way ANOVA and Tukey multiple comparisons, or (D-H) 1-way ANOVA and Dunnett's multiple comparisons (n=4).

Author Manuscript Author Manuscript Author Manuscript Author Manuscript

Author Manuscript

Author Manuscript

Author Manuscript

Author Manuscript

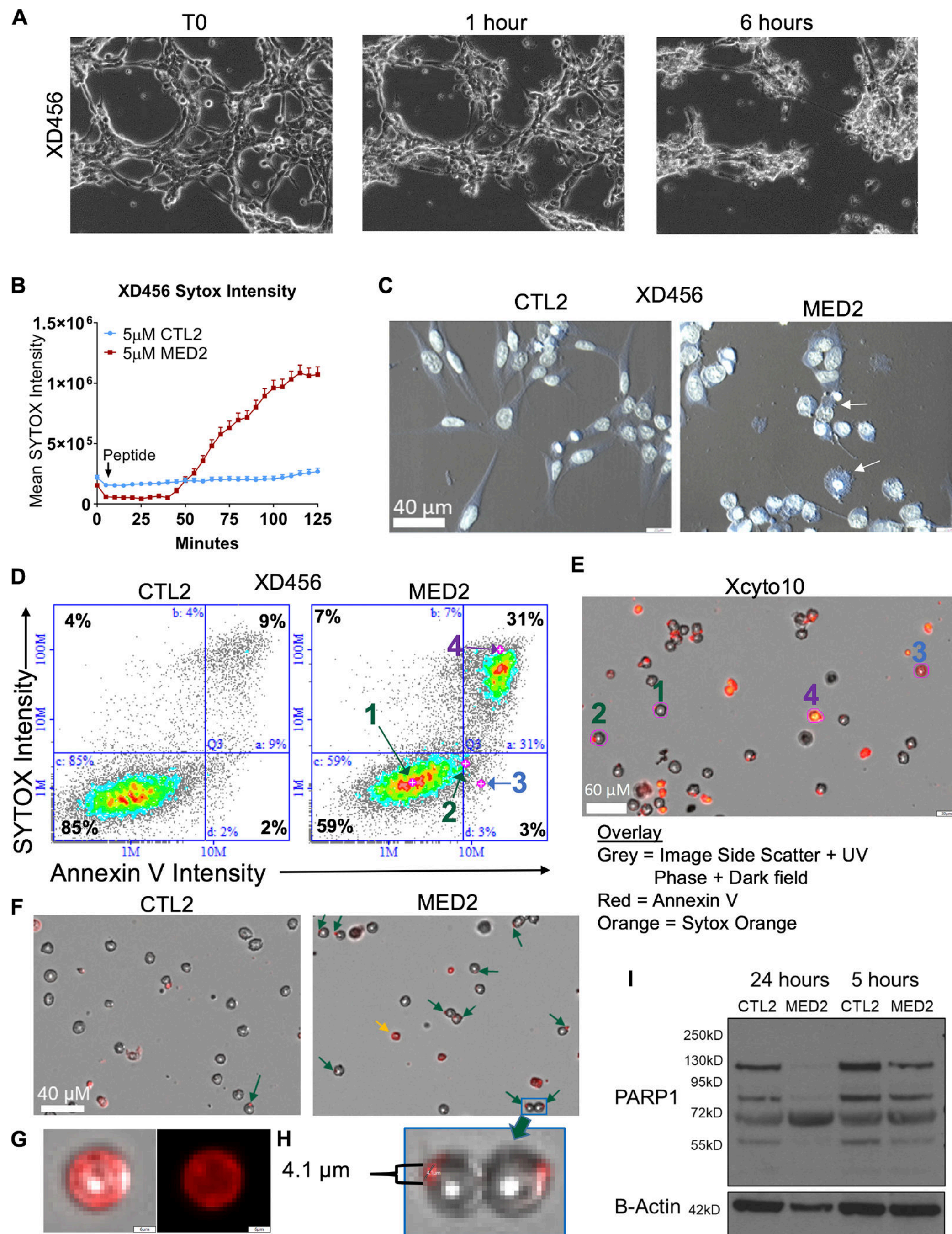

Figure 2.

MED2 is similarly cytotoxic to adherent or suspension cells and induces cytoplasmic retraction and Annexin-V positive blebbing. **(A)** Still frames from time course treatment of XD456 with 3µM MED2 (EVOS AMG, 10X). **(B)** Mean SYTOX intensity per cell of XD456 treated with 5µM CTL2/MED2 over 125 minutes (5-minute intervals, CellInsight CX7, n>400 cells). **(C)** Image of XD456 morphology 3 hours after 3µM CTL2/MED2. Arrow depicts membrane blebbing and retraction of cellular processes (Xcyto10, 20X). **(D)** Apoptosis assay of XD456, 5 hours after 3µM CTL2/MED2, showing Annexin-V intensity

Author Manuscript Author Manuscript Author Manuscript Author Manuscript

(X-axis) SYTOX intensity (Y-axis) (**E**) Individual selected cells (pink outline, numbered 1–4) in XcytoView are identifiable in (**D**) scatterplot data indicated by pink crosses. **(F)** Increases in Annexin-V intensity of Annexin-$V^{negative}$/$SYTOX^{negative}$ cells was due to the formation of Annexin-V positive blebs (green arrow), which differs from an Annexin-$V^{positive}$ cell (yellow arrow). **(G)** Zoomed view of Annexin-V positive cells (phase contrast and Annexin-V overlay left, Annexin-V only right) and (**H**) Annexin-V blebs, averaging 1–5μm (phase contrast/Annexin-V overlay). (**I**) Effects of 3μM MED2 on PARP1 cleavage in XD456 at 5 and 24 hours post-treatment **(D-H)** (Xcyto10, 4X). (**B**) Mean ± SEM.

Author Manuscript

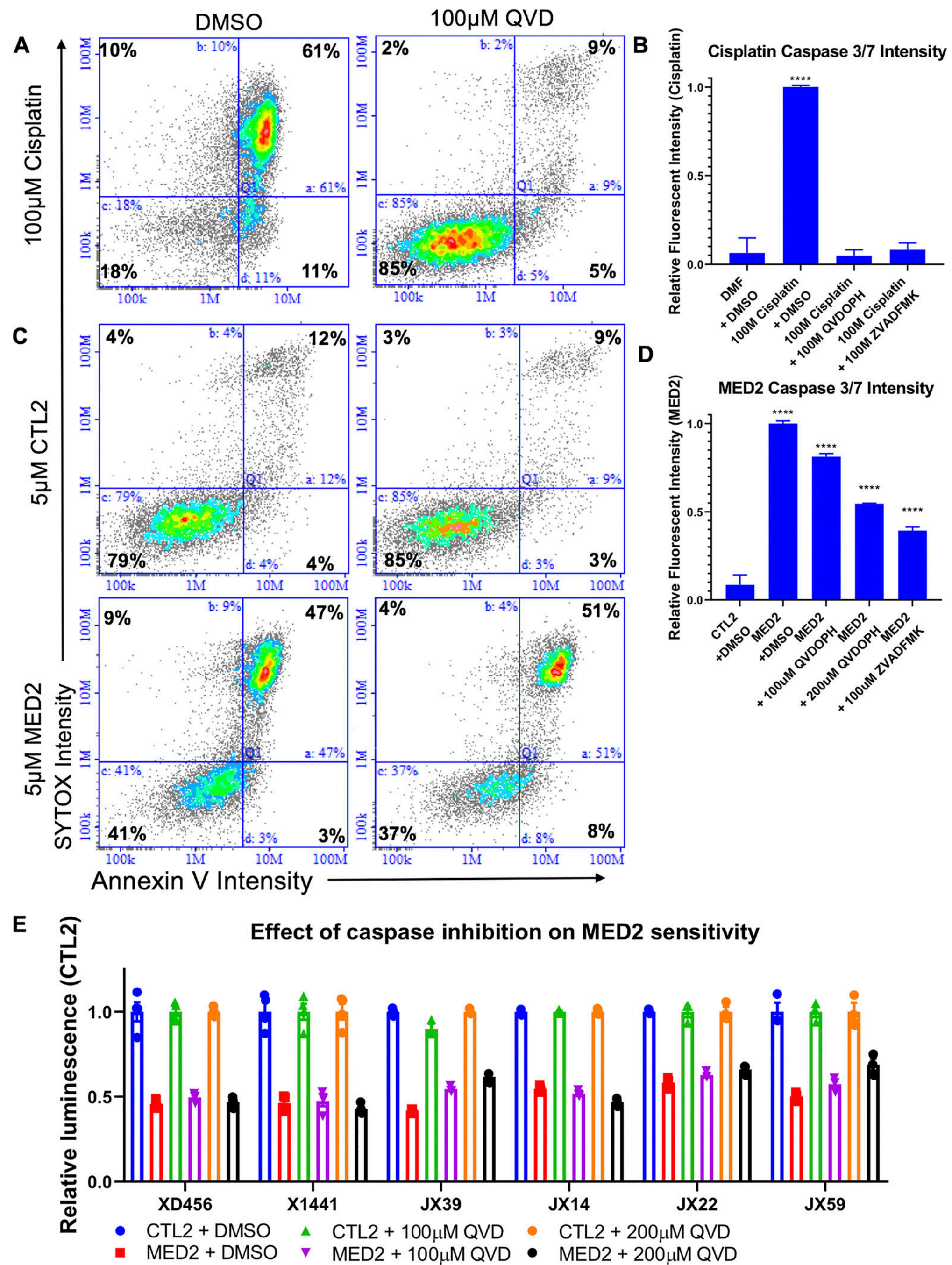

Figure 3.

MED2 cytotoxic effects are resistant to caspase inhibition. **(A & B)** X1441 cells pretreated with 100μM QVDOPH (QVD) or DMSO overnight before 100μM Cisplatin treatment for 24 hours. **(A)** Apoptosis assay depicting caspase inhibition blocking cisplatin's cytotoxicity. **(B)** Suppression of caspase 3/7 activation by caspase inhibitors measured as mean fluorescent intensity per cell relative to cisplatin treatment (n>5000). **(C)** 5μM MED2 induced substantial increases in Annexin-V^{positive} / SYTOX^{positive} cells after 9 hours compared to CTL2, and 100μM QVDOPH has no protective effects. **(D)** MED2 triggered increases in

caspase 3/7 activation relative to CTL2, but 1–200μM QVDOPH or 100μM Z-VAD-FMK could not entirely block caspase activation (n>5000). (**E**) Relative viability of cells treated with MED2/CTL2 near their GI50's after 5 hours and pretreatment of 100μM or 200μM QVDOPH (n=3). XD456 and X1441 treated at 2.5μM & JX14, and JX39 treated at 5μM. All scatterplots generated in Xcytoview. Gating and compensation settings in Supplementary Figures S3 & S6. (**B, D, E**) Relative Mean ± SEM. 2-way ANOVA and Tukey's multiple comparison test.

Author Manuscript Author Manuscript Author Manuscript Author Manuscript

Author Manuscript
Author Manuscript
Author Manuscript
Author Manuscript

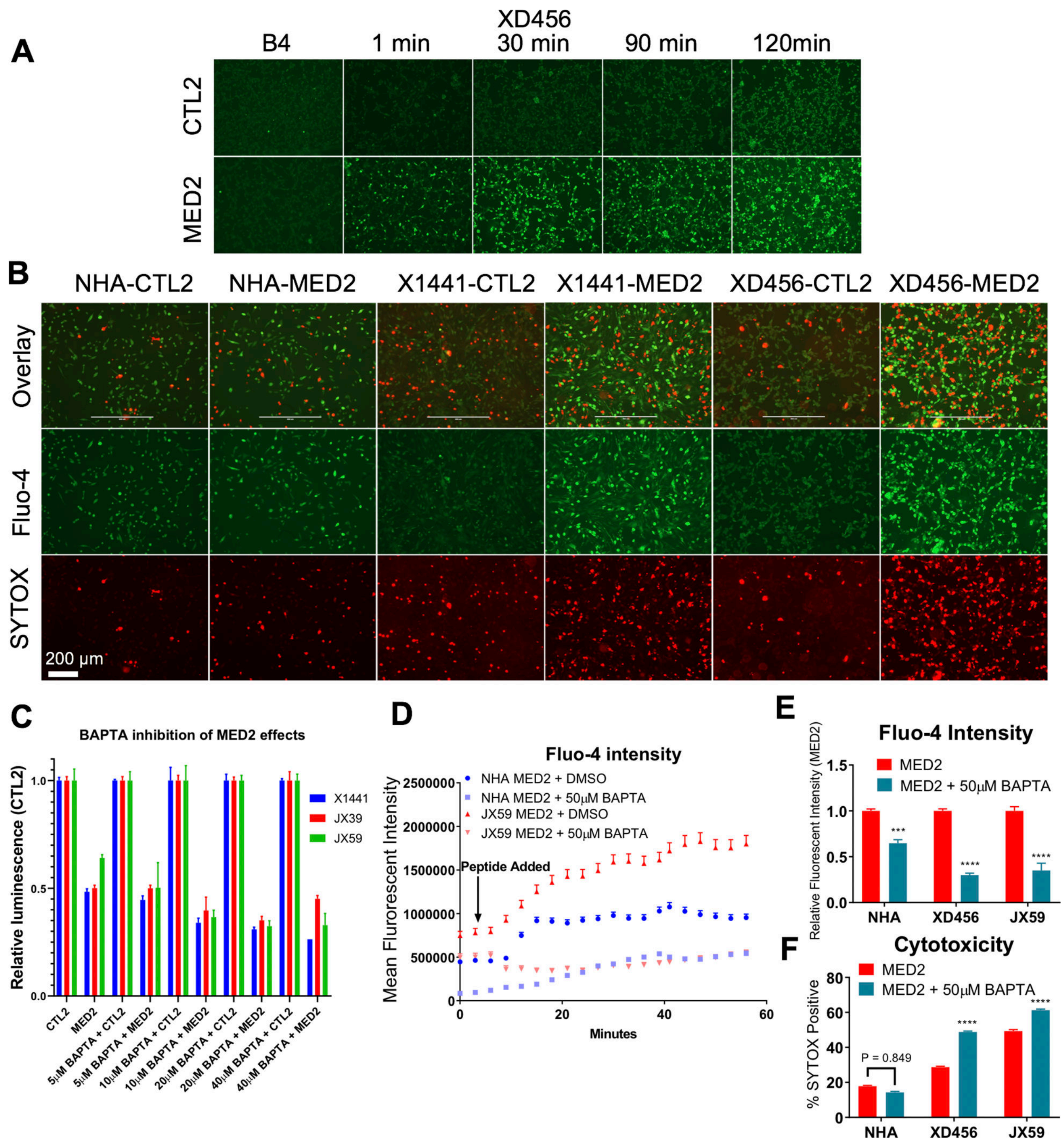

Figure 4.

TAT-ED mimetic triggers rapid and sustained increases in intracellular calcium in GBM as compared to NHAs. **(A)** Serial images of XD456 Fluo-4 fluorescence after treatment with 3µM CTL2 or MED2. B4 = before peptide. Greater Fluo-4 fluorescence corresponds with increased intracellular calcium. **(B)** NHAs, X1441, and XD456 imaged 1.5 hours after 3µM CTL2/MED2 and co-stained with SYTOX (AMG EVOS, 10X). **(C)** Relative viability of X1441 (Proneural), JX39 (Classical) and JX59 (Mesenchymal) pretreated with BAPTA before 5-hour treatment with CTL2/MED2. **(D)** Mean Fluo-4 intensity of JX59 and NHAs

Author Manuscript Author Manuscript Author Manuscript Author Manuscript

over 1 hour with pretreatment of 50μM BAPTA or DMSO, and 3μM MED2 (CellInsight CX7 LZR, 4X, 3 min intervals). **(E)** Mean Fluo-4 intensity per cell and **(F)** percentage of SYTOX positive cells pretreated with 50μM BAPTA and MED2/CTL2 treatment for 1.5 hours (Xcyto10, 4X). (C-F) Cells treated near GI50 with XD456 and X1441 at 2.5μM, and JX39 and JX59 at 5μM peptide. 2-way ANOVA and Tukey's multiple comparison test.

Author Manuscript Author Manuscript Author Manuscript Author Manuscript

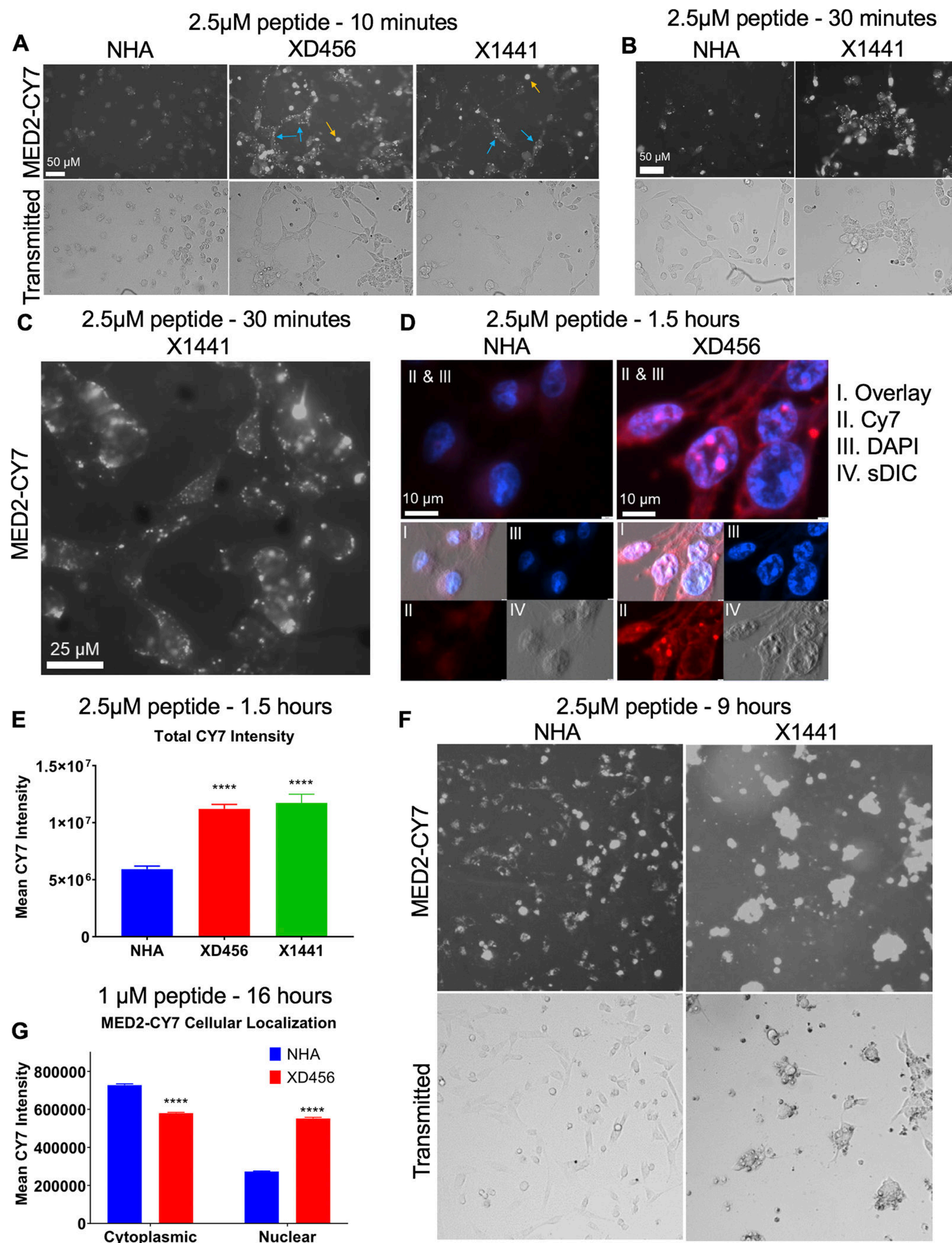

Figure 5.

MARCKS TAT-ED mimetic binds in a punctate manner near the plasma membrane and preferentially accumulates inside GBM *in vitro*. **(A-G)** Adherent cells treated with 2.5μM MED2-CY7 at indicated time points. **(A)** Live cell imaging of NHAs, XD456 and X1441 10 minutes post-treatment, with punctate MED2 accumulations seen at the plasma membrane (blue arrow) and dead cells (orange arrow) (AMG EVOS; 10X). **(B)** Punctate accumulations of MED2-CY7 in NHAs and X1441 after 30 minutes of treatment (AMG EVOS; 10X). **(C)** Close-up of X1441 CY7 accumulations at 30 minutes (AMG EVOS; 20X). **(D)** Images of

Author Manuscript
Author Manuscript
Author Manuscript
Author Manuscript

fixed NHAs and XD456 treated with MED2-CY7 for 1.5 hours. I Overlay; II Red = CY7; III Blue = DAPI; IV Grey = simulated differential interference contrast (Xcyto10; 20X; 800% digital zoom). **(E)** Quantification of mean CY7 fluorescent intensity in fixed NHAs, XD456, and X1441 after 1.5 hours MED2-CY7 (Xcyto10, 20X). **(F)** MED2 accumulations in NHAs and X1441 after 9 hours (AMG EVOS; 10X). **(G)** Quantification of 1μM MED2-CY7 nuclear and cytoplasmic accumulation after 16 hours (Xcyto10, 20X). **(E)** one-way ANOVA with Dunnett's multiple comparison test. **(G)** two-way ANOVA with Tukey's multiple comparison test. (A, B, C & F) Transmitted light image settings in the supplement.

Author Manuscript

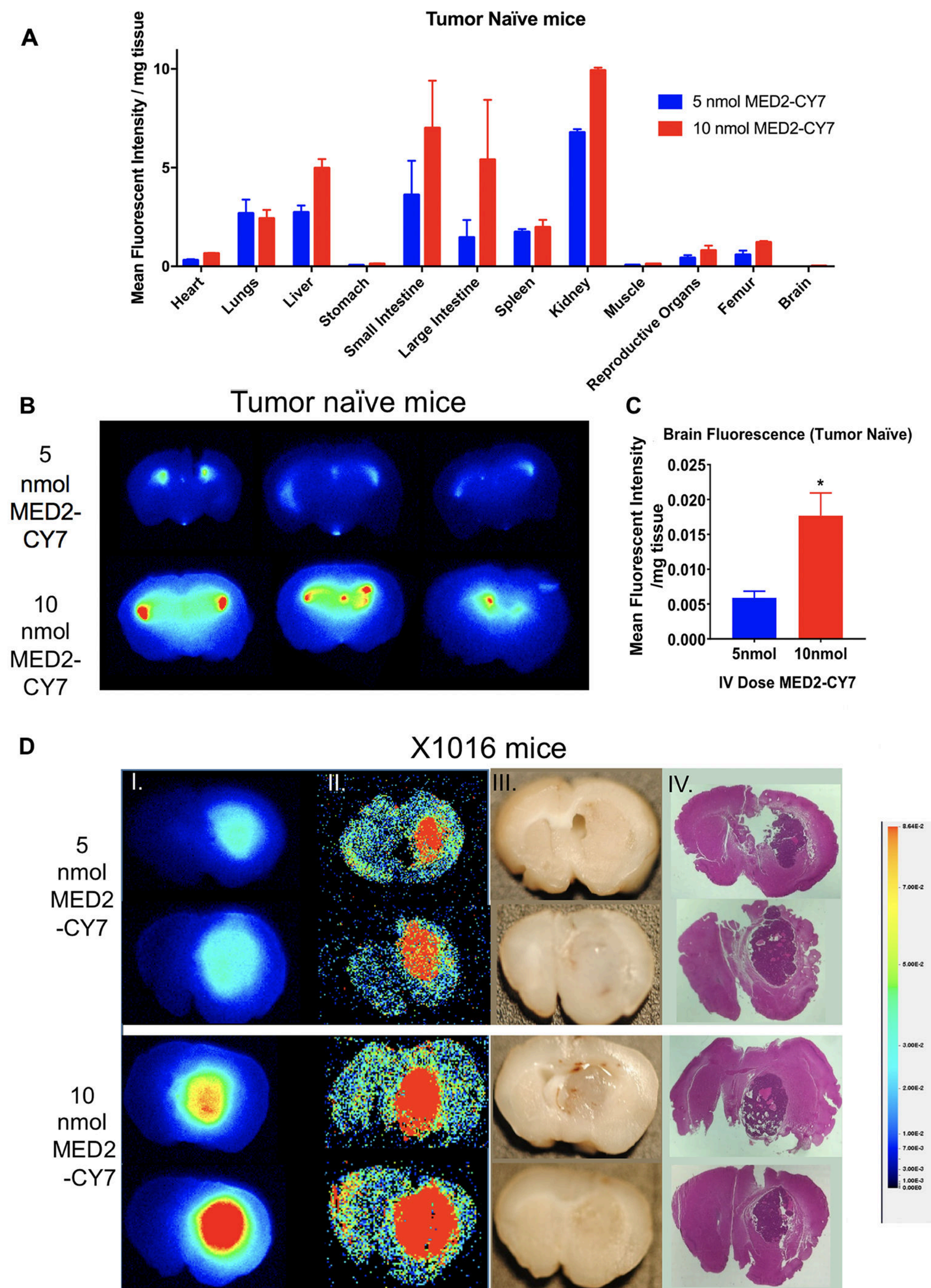

Figure 6.

MED2 crosses the blood-brain barrier concentrating in periventricular brain regions of tumor naïve mice or orthotopic-implanted tumors. **(A-D)** Six-week-old athymic nude mice injected via tail vein with 5nmol (28.3μg) or 10nmol (56.6μg) of MED2-CY7 diluted in normal saline and sacked 3 hours post-treatment. Biological distribution of intravenously delivered MED2-CY7 (**A**) All major organs (except the brain) were collected and weighed and had their fluorescent intensity measured fresh, immediately after dissection using a closed-field fluorescence imaging system (LI-COR Pearl). Tissue thickness was maintained 3–6mm and

Author Manuscript

Author Manuscript

Author Manuscript

Author Manuscript

all tissues were normalized by weight. (n=3 per dose group) (Mean ± SEM) (**B**)The brain was formalin fixed overnight before coronal sectioning (5 mm) and fluorescent imaging performed (Pearl imaging). **(B)** Gross images of CY7 fluorescent intensity of coronal sections (5 mm) of the brain from six tumor naïve mice (Pearl Imaging). **(C)** Quantification of fluorescent intensity (Pearl imaging) per mg tissue of 5nmol and 10nmol treated mice (n=3) (Mean ± SEM). **(D)** Images of serial sections from implanted X1016 PDX into the brain. CY7 fluorescence imaging of (I) 5mm coronal slices (Pearl imaging), and (II) mounted slice (Odyssey CLx). Light imaging of (III) gross brain and (IV) hematoxylin and eosin stained slide. Gross and fluorescence images are the same slice and the color scale maintained for each instrument. Color bar represents Pearl imaging (I). Mounted slides are consecutive sections.